Propagator nonlocalities in nuclear photopion reactions

G. Toker* and F. Tabakin
Department of Physics and Astronomy, University of Pittsburgh, Pittsburgh, Pennsylvania 15260
(Received 18 August 1982)

The coordinate-space distorted-wave impulse approximation approach to (γ,π) and (π,γ) reactions on light nuclei is extended to include the full nonlocality of the pion, nucleon, and isobar propagators that appear in the photoproduction operator. Whereas the introduction of the pion-propagator nonlocality always produces a large effect on the corresponding term of the nuclear photopion amplitude, the other nonlocalities affect mainly the relative phases of the appropriate contributions leaving their magnitude almost unchanged. As a result, in a nucleus like ^{12}C, where at low energies one diagram (the contact term) accounts for most of the cross section and the pion-pole term is not very important, there is almost no change compared with the local calculation. On the other hand, in the nuclei ^{13}C and ^{15}N, where an appreciable interference occurs between the contact and pion-pole diagrams, the nonlocality effect is quite large. Particularly affected is the reaction on the nucleus ^{14}N, even at very low energies. Our treatment blends coordinate- and momentum-space techniques and hence allows one to incorporate other effects such as medium corrections or pion-nucleon form factors. Comparison with available data is also discussed.

[NUCLEAR REACTIONS (γ,π) and (π,γ) calculations for ^{14}N, ^{12}C, ^{13}C, and ^{15}N.]

I. INTRODUCTION

The coordinate-space distorted wave impulse approximation (DWIA) approach has provided a generally good description of low-energy reactions of pion photoproduction[1,2] and radiative capture[3,4] on light nuclei. Successful calculations carefully incorporate the following basic "ingredients": accurate description of the high momentum transfer characteristics of nuclei (through many-body matrix elements of single-nucleon operators, correlated whenever possible with electron scattering data), pion-nucleon optical-model wave functions (consistent with pion-nucleus data), and an operator to describe pion photoproduction on a single nucleon. We wish also to point out that in photopion reactions the DWIA is a much better approximation than in, say, pion-nucleus scattering, owing to the weakness of the electromagnetic processes in the initial state. There is no need, so far, for second-order electromagnetic processes, while the strong final-state interactions are included to all orders in the pion-nucleus distorted waves. (A more serious approximation is the restriction to only one-body nuclear operators, so that "one-body operator approximation" is perhaps a more appropriate name.) The main appeal of DWIA (or, rather, of OBOA) is that the relatively simply physical picture of the process, of the pion being photoproduced from a nucleon in the nucleus and then making its way outside, is implemented through a detailed microscopic calculation essentially without adjustable phenomenological parameters. More complicated physical processes can be taken into account partially by suitably modifying single-nucleon processes or, at a later stage, through two- and more-body operators.

Recent photopion experiments,[5] however, revealed some serious discrepancies with calculations for selected nuclei, which suggests that the conventional local one-body operator approach (OBOA) has to be refined. In addition to addressing these discrepancies, it is important to extend the energy range of the OBOA calculations to the 3,3 resonance region where experiments with neutral and charged pions are under way.[6] In this region, medium-propagator and, possibly, exchange-current corrections are expected to become important. Before any of these interesting effects are incorporated, however, one should remove all nonessential approximations from the present formulation. By far the most serious of these approximations is the local (pointlike) treatment of the photoproduction operator. As a bonus, once the nonlocality of the operator is restored, any corrections that are effective one-body operators become easy to incorporate.

In this paper we extend the earlier Pittsburgh photopion calculations[2,4] to take into account the full nonlocality of the elementary photoproduction operator. We develop our nonlocality formalism for the Blomqvist-Laget[7] (BL) operator which has an appealing physical interpertation and is very convenient for nuclear applications. Our method, however, is quite general and can be applied to any operator. It consists in treating the elementary photoproduction step of the process in the momentum rather than coordinate space. We regard this work as a first step towards a new generation of γ,π calculations that will remove numerous currently accepted approximations and restrictions, some of which are discussed below; any such improvement requires momentum-space techniques. At the same time we preserve the reliability and physical clarity of coordinate-space distorted-wave calculations.

In Sec. III we present our method for restoring nonlocality to the separate terms of the BL operator. The main

advantage of our procedure is that it yields simple replacement formulae for the nucleon orbitals and pion distorted waves entering the local calculation. As a consequence, our treatment is a "local-equivalent" one and requires minimal changes in the local technique. Effectively, the relevant part of the calculation is performed in momentum space, which opens a natural way to incorporate medium effects. For computational ease, we replace the optical-model pion-nucleus wave functions by phase shift equivalent separable-model wave functions that reproduce the behavior of the original optical wave functions in the inner region. These wave functions are discussed and compared to the optical functions in Appendix A. We also point out the dependence of photopion reactions on the behavior of pion waves inside nuclei and the general need for more reliable pion-nucleus wave functions.

In Sec. IV, we discuss the results for the reaction $^{14}\mathrm{N}(\gamma,\pi^+)^{14}\mathrm{C}_{\mathrm{g.s.}}$ at pion laboratory kinetic energies $T_\pi=20$, 50, and 120 MeV. Here the photoproduction amplitude is largely the result of a destructive interference between the Kroll-Ruderman term $\vec{\sigma}\cdot\vec{\epsilon}$ and the pion-pole term and thus is very strongly affected by the introduction of nonlocalities. While the nonlocalities of the nucleon and Δ diagrams result in relatively small perturbations, that of the pion-pole term is always large. This means that the local limit for the pion-pole diagram is simply incorrect. The effect of the nonlocality on the intermediate-baryon diagrams is mainly to introduce an additional complex phase without appreciably changing the magnitude of their contributions. This (angle-dependent) phase can be qualitatively understood as the factor $e^{i\vec{p}\,\vec{r}}$ picked up when the intermediate particle with momentum p is allowed to propagate over the distance r. The inclusion of nonlocality reveals an interesting difference between the pseudoscalar (PS) pion-nucleon coupling γ_5 and the derivative or pseudovector (PV) coupling $\gamma_5\partial\!\!\!/$: In the PS coupling, the usually dominant Kroll-Ruderman term originates from the nucleon (or crossed-nucleon) diagram, has a propagator and is thus affected by the nonlocality. In the PV coupling, this term is primarily due to the contact (seagull) diagram which is, of course, strictly local. For single-nucleon pion photoproduction, the two couplings are largely equivalent since they produce the same Kroll-Ruderman low-energy limit and differ only in more complicated spin- and orbital angular momentum-dependent operators that are small compared with the $\vec{\sigma}\cdot\vec{\epsilon}$. A nucleus, however, often acts as a "resonating cavity" for angular momentum operators, suppressing some and picking up others; as a result, small terms of the photoproduction operator and the difference between the two couplings may be considerably enhanced. Good examples of such behavior are the nuclei ^{14}N, ^{13}C, and ^{15}N, as discussed in Secs. IV and V.

As an example of medium effects and with the pion condensation[8] in mind, we use the nonlocality technique to test the "softening" of the in-the-medium pion by arbitrarily giving it a smaller mass. An an outgrowth of such calculations, we feel that the nucleus ^{14}N may prove to be a more interesting testing ground for the ideas of pion condensation than ^{13}C because of the unusual prominence that the pion-pole term has in ^{14}N even near threshold. Of course, meson-exchange currents have to be taken into account before any definite conclusions about pion condensation can be drawn. We stress that a proper incorporation of medium effects must follow a carefully organized procedure[9] to incorporate fully dressed propagators and vertices avoiding overcounting, and, for lack of off-mass-shell pion wave functions, should employ different pion distorted waves for the long- and short-range parts of the photoproduction operator.[10]

In Sec. V, we compare the local and nonlocal calculations for other nuclei: pion photoproduction on ^{12}C and ^{13}C and pion radiative capture on ^{15}N and ^{13}C. In ^{12}C there is very little difference between the local and nonlocal results except in the resonance region ($T_\pi=140$ MeV). In this nucleus the reaction is dominated by the $\vec{\sigma}\cdot\vec{\epsilon}$ term which is affected by nonlocality at most through the additional complex phase; since there is practically no interference with the pion pole or other terms, the influence on the photopion cross section is small. The situation is different in such nuclei as ^{15}N or ^{13}C, where the leading contribution is relatively suppressed. For these nuclei, an interesting interference with the pion-pole term appears,[4] which leads to minima in their differential cross sections. The nonlocality then plays an important role, both by strongly affecting the pion-pole term and by changing the phases of the $\vec{\sigma}\cdot\vec{\epsilon}$ term (in the PS coupling) and of other contributions which tend to fill in the minima. We compare our results with available data. Details of our calculational procedures are relegated to Appendix B.

II. BLOMQVIST-LAGET OPERATOR AND THE DWIA

In our calculations of photopion reactions we make use of the Blomqvist-Laget[7] (BL) operator for the elementary reaction $\mathrm{N}(\gamma,\pi)\mathrm{N}'$. This operator is derived from the lowest-order Feynman diagrams shown in Fig. 1; in addition to providing a physical picture of the process, the BL operator is obtained directly in an arbitrary frame of reference. This latter feature makes this photoproduction operator especially suitable[7] for nuclear applications; an operator obtained with the help of dispersion relations, for example, still has to be transformed from the two-body c.m. frame into the moving frame of the struck nucleon, which is an ambiguous procedure and difficult in view of the inevitable partial-wave decomposition.

Note that embedding the BL operator in a nuclear calculation is also by no means a unique process: Some three-dimensional reduction has to be performed since the operator is meant to operate not only on the three-momenta $\vec{p}$ of the final particles but on their zero com-

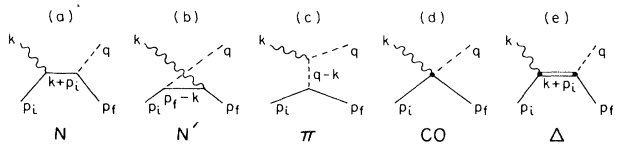

FIG. 1. Lowest order Feynman diagrams for pion photoproduction on nucleons.

ponents p_0 as well. In other words, zero components of particles must be given certain fixed values. We adopt here the view that the relevant particles must be put on their mass shells; e.g., in the pion-pole diagram of Fig. 1(c) we set $(q_\pi)_0=E_q$. It may turn out that some other choice is better than ours; in fact the optimum choice of p_0 in a three-dimensional reduction is a major theoretical problem. Short of a full solution of this problem, our prescription has the advantage that the photoproduction operator has exactly the same form for both plane- and distorted-wave pions.

In general, an operator derived from the first-order Feynman diagrams reflects the interaction Hamiltonian. The Blomqvist-Laget operator, however, is an effective scattering t matrix. Indeed, it includes pion-nucleon final-state interactions by means of the phenomenological Δ term rather than through the pion-nucleon scattering wave function and is directly fitted to (γ,π) data. (Only the 3,3 phase of the resonant multipoles is reproduced; the other, small, phases are ignored.) We wish to point out that the photoproduction operator to be used in nuclear applications should be the photopion interaction Hamiltonian rather than the scattering matrix t. Indeed, when many-body effects are neglected, the distorted-wave Born approximation formula

$$M^{(B)}=\left\langle \psi^{(-)}_{\pi,A'} \middle| \sum_{i=1}^{A} V^{(i)}_{\pi,\gamma} \middle| \chi_A \right\rangle \tag{2.1}$$

becomes exact since the pion rescatterings are already included to all orders in $\psi^{(-)}_{\pi,A'}$. The DWIA formula

$$M^{(I)}=\left\langle \psi^{(-)}_{\pi,A'} \middle| \sum_{i=1}^{A} t^{(i)}_{\pi,\gamma} \middle| \chi_{\gamma,A} \right\rangle \tag{2.2}$$

then double counts the pion interactions with the struck nucleon (already contained in $t_{\pi,\gamma}$). This double counting, however, is only a $1/A$ effect, which explains the general success of the BL operator in nuclear photopion reactions. The above considerations suggest that the Δ term, which turns the BL operator into the t matrix, be dropped. The single-nucleon pion photoproduction then must also be calculated using the single-nucleon analog of formula (2.1). On the other hand, one could argue for the presence of an "elementary" Δ with a fractional coefficient in the operator alongside a purely rescattering Δ in the wave function. Therefore, we perform all our calculations both with and without the Δ term, overcounting and undercounting this contribution. Except for neutral pion photoproduction (not treated in this paper), the resulting error margin proves to be always small. It is only when the Δ "happens" to fill in a minimum created by an interference between other terms, which occurs for instance in ^{13}C and ^{15}N, that it plays any appreciable role. Note that we do not argue against the physical effect of creation and propagation of the isobar. This effect is fully contained in the pion-nucleus scattering wave function $\psi^{(-)}_{\pi,A'}$.

Another theoretical uncertainty results from the choice of the PS or PV pion-nucleon coupling: From a practical viewpoint one cannot reject the PV coupling simply because of its nonrenormalizability [or because the strictly local contact term of Fig. 1(d) defies our physical intuition] nor prefer it because it directly produces a vector current, since the single-nucleon data are described equally well by both couplings. Even though the PV coupling apparently leads to a better description of the π^0 photoproduction near threshold,[11,7] this "success" is somewhat misleading: The low-energy π^0 photoproduction proceeds through "small" terms of the BL amplitude (the dominant terms are proportional to the pion charge), and these terms cannot be expected to be reliable. In fact, most of the small multipoles are not reproduced well in either coupling.[7] We emphasize that the deficiency is only in the small terms: these, however, may become important when the energy is increased to the resonance region. Until a better photoproduction operator is available, we regard the difference between the PV and PS results an another reflection of the theoretical uncertainty.

III. MOMENTUM-SPACE OPERATORS IN A COORDINATE-SPACE CALCULATION

A. Pion-pole term

Each of the diagrams of Fig. 1, except the contact term of Fig. 1(d), contains a propagator with the denominator $1/(p^2-m^2)$, where p and m are the four-momentum and mass of the intermediate particle. Coordinate-space calculations, typically,[2,4] replace these propagators by their zero-momentum limits, which leads to local objects. Possible momentum terms in the numerator are, however, transformed into appropriate derivatives. In order to restore the nonlocalities (to correct the treatment of the denominators), we introduce the nonlocality "smearing" operator

$$\Omega(\vec{x}-\vec{x}\,')=\left\langle \vec{x} \middle| \frac{1}{p^2-m^2} \middle| \vec{x}\,' \right\rangle , \tag{3.1}$$

which is simply the Fourier transform of the propagator. We are careful to always choose the photon vertex to be to the right of the operator (3.1). The photon, being a plane wave, can then be viewed as "shifted" to the other side of the propagator, as illustrated in Fig. 2. The operator Ω then acts only on one function: a nucleon orbital for the diagrams of Figs. 1(a), 1(b), and 1(e) or the pion wave function for the diagram 1(c). Instead of just one value $x'=x$ of this function, an integration over all possible values of x' appears, hence the name smearing. For the pion-pole diagram of Fig. 1(c), for example, we readily obtain

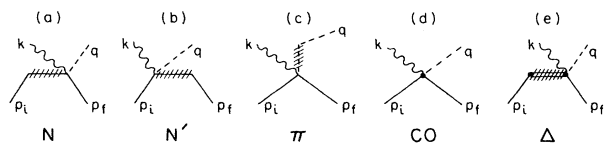

FIG. 2. Local equivalent picture of the nonlocal diagrams of Fig. 1 in our formalism. The hatched lines correspond to smeared functions.

$$\Omega^{(\pi)}(\vec{x},\vec{x}\,')=-2E_{q_0}k\int\frac{d^3q}{(2\pi)^3}\frac{e^{i\vec{q}\cdot(\vec{x}-\vec{x}\,')}}{(q-k)^2-m_\pi^2}$$

$$=E_{q_0}k\int\frac{d^3q}{(2\pi)^3}\frac{e^{i\vec{q}(\vec{x}-\vec{x}\,')}}{kE_q-\vec{k}\vec{q}}\ . \tag{3.2}$$

The on-shell pion energy E_{q_0} in front ensures that in the "old" local limit $E_q\to E_{q_0}$, $\vec{q}\vec{k}\to 0$ the operator becomes the delta function $\delta(\vec{x}\,'-\vec{x})$.

Note that in using the free-space BL operator we have relied implicitly on momentum conservation, or on translational invariance, which is only an approximation in finite nuclei. We feel, however, that it is reasonable to assume local translational invariance since medium corrections can be introduced as a next step. Note also that in (3.2) we have canceled the masses of the intermediate and outgoing pions: The pion produced in the diagram of Fig. 1(c) is still in the medium and its wave function will be distorted on the way out; medium corrections to the mass can be thought to be contained in the optical potential. Hence, any medium modification of the pion mass m_π should only change the energies E_q and E_{q_0}. This procedure is necessarily arbitrary; we find it more to our taste than, say, attributing the free-pion mass to the produced particle and the in-the-medium mass to the virutal pion. In any case, medium effects are investigated here only for order-of-magnitude estimates.

Our nonlocality algorithm consists in replacing the pion distorted wave function $\psi_\pi(\vec{x})$ by the smeared wave [cf. Fig. 2(c)]

$$\tilde{\psi}_\pi(\vec{x})=\int d^3x'\Omega^{(\pi)}(\vec{x},\vec{x}\,')\psi_\pi(\vec{x}\,')\ . \tag{3.3}$$

The remaining parts of the diagram are unchanged compared with the local limit and the earlier calculation is modified in a minimal way. We now rewrite (3.2) and (3.3) in the following form:

$$\tilde{\psi}_\pi(\vec{x})=E_{q_0}\int\frac{d^3q}{q}\frac{e^{i\vec{q}\cdot\vec{x}}}{(2\pi)^3}\frac{1}{E_q/q-\hat{\vec{q}}\cdot\hat{\vec{k}}}\psi_\pi(\vec{q})\ , \tag{3.4}$$

where $\hat{\vec{q}}$ and $\hat{\vec{k}}$ are the unit vectors and $\psi_\pi(\vec{q})$ is the pion distorted wave in momentum space. Finally, we perform a partial-wave decomposition with the result

$$\tilde{\psi}_\pi(\vec{x})=\sum_{l,m}\left[\frac{2}{\pi}\right]^{1/2}i^l\tilde{\psi}^{(\pi)}_{l,m}(x)Y_{l,m}(\hat{x})\ , \tag{3.5}$$

$$\tilde{\psi}^{(\pi)}_{l,m}(x)=(-)^m\sum_{l_1L}(2L+1)[(2l+1)(2l_1+1)]^{1/2}\begin{bmatrix}l_1 & L & l\\ m & 0 & -m\end{bmatrix}\begin{bmatrix}l_1 & L & l\\ 0 & 0 & 0\end{bmatrix}Y^*_{l_1m}(-\hat{q}_0)I^{(\pi)}_{lLl_1}(x)\ , \tag{3.6}$$

where $\vec{q}_0$ is the actual (asymptotic) momentum of the outgoing pion relative to which the original distorted wave $\psi_\pi(\vec{x})$ is expanded, and the radial integral is

$$I^{(\pi)}_{lLl_1}(x)=E_{q_0}\int_0^\infty q\,dq\,j_l(qx)Q_L\left[\frac{E_q}{q}\right]\psi_{l_1}(q)\ ; \tag{3.7}$$

j_1 and Q_L are, respectively, the spherical Bessel function and the Legendre function of the second kind, and $\psi_{l_1}(q)$ is the unsmeared partial wave in momentum space. We have made use of the expansion

$$\frac{1}{z-\hat{q}\cdot\hat{k}}=4\pi\sum_L Q_L(z)Y_L(\hat{q})\cdot Y_L(\hat{k}) \tag{3.8}$$

and chose the photon to move along the z axis:

$$Y_{LM}(\hat{\vec{k}})=\delta_{M,0}\left[\frac{2L+1}{4\pi}\right]^{1/2}\ . \tag{3.9}$$

Note that the smeared pion wave $\tilde{\psi}_\pi(\vec{x})$ is no longer cylindrically symmetric with respect to $\vec{q}_0$. This symmetry, however, is of no use in photopion reactions anyway (by contrast with pion elastic scattering) since the incident particle, the photon, is different from the scattered one, so that the summation over the pion magnetic quantum number is performed explicitly even in the local limit.[2] The smeared partial waves (3.6) thus directly replace the original partial waves $\psi^{(\pi)}_l(x)$ whenever the contribution of the pion-pole diagram is evaluated.

The main physical effect incorporated in the mathematical expression (3.6) is the mixing of partial pion waves resulting from the fact that, in contrast with the local picture, the photon is actually absorbed "away" from the nucleon. The new summation variable L is, in effect, the angular-momentum transfer arising from this "lever-arm" effect.

Evaluation of the momentum-space integral (3.7) requires knowledge of the pion partial wave functions in momentum space, which entails several difficulties. For instance, the Coulomb tail is very difficult to treat (this can be partially circumvented using the Vincent-Phatak method[12]) and, in general, the Fourier-Bessel transform is not easy to perform numerically. Moreover, our previous calculations[2,4] made use of the Michigan State University (MSU) optical potential[13] which contains the $\vec{\nabla}\cdot\rho\vec{\nabla}$ term and hence cannot be transformed into a bounded momentum-space operator without an arbitrary cutoff. At this stage, we felt it appropriate, both for computational ease and also to explore the uncertainty in the pion distorted waves, to construct separable-model pion-nucleus wave functions that are phase equivalent to the original optical functions and reproduce their behavior in the inner region as well as possible (we refer to them below as "mock" functions). The main difference between the optical-potential and mock wave functions is that the latter are generated from potentials with a higher degree

of nonlocality and that their derivatives are smooth, unlike those of the MSU wave functions. With these mock pion waves, the requisite integral (3.7) can be calculated in a rather straightforward way. The mock wave functions are described and discussed in some detail in Appendix A; some numerical aspects of the calculations are relegated to Appendix B.

Let us note, that in the case of plane-wave pions the smeared pion wave function is easily obtained from (3.4) as the product

$$\tilde{\psi}_\pi^{\rm PW}(\vec{x})=\frac{E_{q_0}/q_0}{E_{q_0}/q_0-\cos\theta}\psi_\pi^{\rm PW}(\vec{x})\ , \tag{3.10}$$

where θ is the angle between the photon and the outgoing pion and

$$\psi_\pi^{\rm PW}(\vec{x})=(2\pi)^{-3/2}e^{i\vec{q}_0\cdot\vec{x}} \tag{3.11}$$

is the original plane wave. The nonlocality of the pion-pole term in this case reduced to an angle-dependent factor which tends to build up the forward angles, thereby shifting the pion-pole peak in the differential cross section, and to increase the pion-pole contribution in general. For $T_\pi=50$ MeV pions, $E_{q_0}/q_0=v^{-1}\simeq 1.5$, which leads to a factor of 3 at $\theta=0°$ or a factor of 2 at 45° in the photoproduction amplitude. For distorted-wave pions, the nonlocality effect is more complicated, as will be seen from the explicit calculations presented below. Most cases, however, can be qualitatively understood in terms of the simple factor of Eq. (3.10). The angle dependence of this factor is another illustration of the additional angular-momentum transfer L (lever-arm effect) discussed above. At low energies, the sum (3.8) over L converges quite rapidly, since then the inverse pion velocity $v^{-1}=E_q/q$ is large and the Legendre functions Q_L quickly decrease with growing L. On the other hand, when q becomes large (and such q's play an increasingly important role at higher energies), the argument v^{-1} becomes close to unity and more values of L are required. The plane-wave factor in (3.10) also becomes very large: at $T_\pi=200$ MeV, it is 11 at $\theta=0°$ and 2.8 at $\theta=45°$. The effect is amplified when the pion mass is softened: For a very small m_π, the pion becomes highly relativistic and the factor (3.10) is always important. Already from these plane-wave estimates we can see the importance of the nonlocality of the pion propagator.

B. Baryon diagrams

Smearing of the nucleon diagram of Fig. 1(a) is performed in a way analogous to that of the pion-pole diagram. Again, the photon is shifted to the other vertex and the nucleon orbital

$$\psi_{nl\mu}(\vec{x})=R_{nl}(x)Y_{l\mu}(\hat{\vec{x}}) \tag{3.12}$$

is replaced by a smeared wave function

$$\begin{aligned}\tilde{\psi}_{nl\mu}(\vec{x})&=\int d^3x'\,m_N k\int\frac{d^3p}{(2\pi)^3}\frac{e^{i\vec{p}\cdot(\vec{x}-\vec{x}')}}{kE_p-\hat{\vec{p}}\cdot\hat{\vec{k}}}\\&\quad\times\psi_{nl\mu}(\vec{x}')\\&=\sum_{l_1\mu_1 L}\langle lL\mu 0\,|\,l_1\mu_1\rangle\tilde{R}_{n,lLl_1}(x)Y_{l_1\mu_1}(\hat{\vec{x}})\ ,\end{aligned} \tag{3.13}$$

where

$$\begin{aligned}\tilde{R}_{n,lLl_1}(x)&=i^{l_1-l}(-)^{l-L}(2L+1)\sqrt{2l+1}\\&\quad\times\begin{bmatrix}l & L & l_1\\ 0 & 0 & 0\end{bmatrix}I^{(N)}_{n,lLl_1}(x)\end{aligned} \tag{3.14}$$

and

$$\begin{aligned}I^{(N)}_{n,lLl_1}(x)&=m_N\left[\frac{2}{\pi}\right]^{1/2}\int_0^\infty p\,dp\,j_{l_1}(px)\\&\quad\times Q_L\left[\frac{E_p}{p}\right]R_{nl}(p)\ .\end{aligned} \tag{3.15}$$

The orbitals $R_{nl}(x)$ are, as usual, harmonic-oscillator eigenfunctions and the Fourier-Bessel transform for them

$$R_{nl}(p)=\left[\frac{2}{\pi}\right]^{1/2}\int_0^\infty j_l(px)R_{nl}(x)x^2dx \tag{3.16}$$

is performed analytically.

In the local limit, the sum over the nucleon magnetic quantum number μ is performed analytically, making use of the irreducible-tensor property (3.12). With the introduction of nonlocality, this transformation law is replaced by a slightly more complicated rule (3.13), and some of the angular momentum algebra has to be redone. We start with the nuclear matrix element of some tensor operator t^J [originating in the diagram of Fig. 1(a)], write it in the second-quantized notation, and insert the smeared orbitals (3.13) instead of their local counterparts (3.12),

$$\begin{aligned}\langle J_fM_f\,|\,t^{JM}\,|\,J_iM_i\rangle&=\sum_{\alpha\beta}\langle J_fM_f\,|\,a^\dagger_\alpha a_\beta\,|\,J_iM_i\rangle\langle\alpha\,|\,t^{JM}\,|\,\tilde{\beta}\rangle\\&\equiv\sum_{\alpha\beta}\langle J_fM_f\,|\,a^\dagger_\alpha a_\beta\,|\,J_iM_i\rangle\sum_{l'_\beta\mu'_\beta L}\langle l_\beta L\mu_\beta 0\,|\,l'_\beta\mu'_\beta\rangle R_{n_\alpha l_\alpha}R_{n_\beta,l_\beta Ll'_\beta}\langle l_\alpha s_\alpha\mu_\alpha\sigma_\alpha\,|\,t^{JM}\,|\,l'_\beta s_\beta\mu'_\beta\sigma_\beta\rangle\ .\end{aligned} \tag{3.17}$$

We have followed the notation of Ref. 2 as closely as possible. The single-particle matrix element of t^{JM} appearing last in

the r.h.s of Eq. (3.17) has proper irreducible-tensor properties and is, in fact, identical to the one appearing in the local limit (where, however, $l'=1$ and $\mu'=\mu$). The smearing, therefore, does not depend on the explicit properties of t^{JM} and all the operators that originate in the nucleon diagram of Fig. 1(a) are smeared in the same way. Changing to the *jj* coupling, we obtain after some algebra,

$$\langle J_f M_f \mid t^{JM}_{(D)} \mid J_i M_i \rangle = \sum_{J_1} \langle J_i J_1 M_i M \mid J_f M_f \rangle \sum_{L} \langle J_1 L M_1 0 \mid JM \rangle \langle J_f || t^{JJ_1L}_{(D)} || J_i \rangle \ , \tag{3.18}$$

where D stands for "direct" [referring to the direct diagram of Fig. 1(a) as opposed to the crossed diagram in Fig. 1(b)], and

$$\langle J_f || t^{JJ_1L}_{(D)} || J_i \rangle = \sum_{\alpha\beta} \langle J_f || [a^\dagger_\alpha \times \tilde{a}_\beta]^{J_1} || J_i \rangle \sum_{l'_\beta j'_\beta} (-)^{l'_\beta + s_\beta + L + j_\alpha + J} R_{n_\alpha l_\alpha} \tilde{R}_{n_\beta, l_\beta L l'_\beta}$$

$$\times \langle l_\alpha s_\alpha j_\alpha || t^J || l'_\beta s_\beta j'_\beta \rangle \begin{Bmatrix} l_\beta & s_\beta & j_\beta \\ j'_\beta & L & l'_\beta \end{Bmatrix} \begin{Bmatrix} j_\alpha & j_\beta & J_1 \\ L & J & j'_\beta \end{Bmatrix} \left[\frac{(2j'_\beta+1)(2j_\beta+1)(2j_\alpha+1)(2l'_\beta+1)(2J_1+1)}{2J+1} \right]^{1/2} . \tag{3.19}$$

In the local limit ($L \to 0, \tilde{R} \to R$) this reduces to the result of Ref. 2

$$\langle J_f M_f \mid t^{JM} \mid J_i M_i \rangle = \langle J_i J M_i M \mid J_f M_f \rangle \sum_{\alpha\beta} (-)^{2j_\beta} R_{n_\alpha l_\alpha} R_{n_\beta l_\beta} \left[\frac{2j_\alpha+1}{2j_\beta+1} \right]^{1/2}$$

$$\times \langle J_f || [a^\dagger_\alpha \times \tilde{a}_\beta]^J || J_i \rangle \langle l_\alpha s_\alpha j_\alpha || t^J || l_\beta s_\beta j_\beta \rangle \ . \tag{3.20}$$

In a similar way, *mutatis mutandi,* the expression for the smeared crossed-nucleon diagram of Fig. 1(b) is obtained,

$$\langle J_f || t^{JJ_1L}_{(C)} || J_i \rangle = \sum_{\alpha\beta} \langle J_f || [a^\dagger_\alpha \times \tilde{a}_\beta]^{J_1} || J_i \rangle \sum_{l'_\alpha j'_\alpha} (-)^{l'_\alpha + s_\alpha + j'_\alpha + j_\alpha - j_\beta + J_1} \tilde{R}_{n_\alpha, l_\alpha L l'_\alpha} R_{n_\beta l_\beta}$$

$$\times \langle l'_\alpha s_\alpha j_\alpha || t^J || l_\beta s_\beta j_\beta \rangle \begin{Bmatrix} l_\alpha & s_\alpha & j_\alpha \\ j'_\alpha & L & l'_\alpha \end{Bmatrix} \begin{Bmatrix} j_\alpha & j_\beta & J_1 \\ J & L & j'_\alpha \end{Bmatrix} \left[\frac{(2l'_\alpha+1)(2j_\alpha+1)(2j'_\alpha+1)^2(2J_1+1)}{2J+1} \right]^{1/2} . \tag{3.21}$$

The Δ diagram of Fig. 1(e), finally, is smeared exactly as the direct-nucleon diagram; the only difference is that here the denominator of the propagator is more complicated:

$$D = s - M^2_\Delta \equiv (p_i + k)^2 - M^2_\Delta$$
$$= m^2_N + 2E_{p_i} k - 2\vec{p}_i \cdot \vec{k} - (m_\Delta - i\Gamma)^2 \ , \tag{3.22}$$

where the width Γ must carry some momentum dependence, since for a free Δ it is proportional to the cube of the pion-nucleon c.m. momentum. In a medium, this cubic dependence may be different. Unfortunately, not much is known about the width of the in-the-medium Δ in a model-independent way; it appears that it does not greatly differ from the free-space value.[14] In our application, fortunately, the precise form of the momentum dependence of Γ is not important, since the imaginary part becomes "noticeable" only in the vicinity of the resonance m_Δ itself where the width Γ has its on-shell value Γ_0. The overall effect of the imaginary part is also quite small; it would become appreciable only for unrealistically small widths. In order not to generate higher powers of the cosine in the denominator of (3.13) and thus again make use of the expansion (3.8), we employ the ansatz

$$\Gamma = \Gamma_0 \frac{s - M^2_{N\pi}}{m^2_\Delta - M^2_{N\pi}} \ , M_{N\pi} \equiv m_N + m_\pi \tag{3.23}$$

and neglect Γ^2. [We would have used $\Gamma = \Gamma_0$ with almost the same results. The approach (3.23) is physically more attractive.] This gives

$$D = s - m^2_\Delta + 2i m_\Delta \Gamma_0 \frac{s - M^2_{N\pi}}{m^2_\Delta - M^2_{N\pi}}$$

or

$$D = (1 + i\xi) 2p_i k \left[E_{p_i} + \frac{m^2_N - m^2_\Delta - i\xi(m^2_\pi + 2m_\pi m_N)}{1 + i\xi} - \hat{\vec{p}}_i \cdot \hat{\vec{k}} \right] , \tag{3.24}$$

$$\xi = \frac{2m_\Delta \Gamma_0}{m^2_\Delta - M^2_{N\pi}} \ .$$

The Δ-smeared nucleon orbital is then

$$\tilde{\psi}_{nl\mu}(\vec{x})=(m_N+\mathcal{M})k \times \int\int \frac{d^3p}{(2\pi)^3}\frac{e^{i\vec{p}\cdot(\vec{x}-\vec{x}')}}{k(E_p+\mathcal{M})-\vec{k}\cdot\vec{p}}\psi_{nl\mu}(\vec{x}')d^3x' , \tag{3.25}$$

where

$$\mathcal{M}=\frac{m_N^2-m_\Delta^2-i\xi(m_\pi^2+2m_\pi m_N)}{1+i\xi} , \tag{3.26}$$

and the only change required in the formulae (3.13)—(3.15) is the replacement of the argument of the Legendre function Q_L:

$$\frac{E_{p_i}}{p_i}\rightarrow\frac{E_{p_i}+\mathcal{M}}{p_i} . \tag{3.27}$$

When the cross section is calculated and the sum over nuclear polarizations M_i,M_f is performed, from (3.18) or (3.19) we obtain

$$\bar{\sigma}=F_{\rm kin}\sum_{J_1M}\left|\sum_{JL}\langle J_1LM0\,|\,JM\rangle\langle J_f||t^{JJ_1L}||J_i\rangle\right|^2\frac{(2J_f+1)}{(2J+1)} \tag{3.28}$$

in place of

$$\bar{\sigma}=F_{\rm kin}\sum_{JM}|\langle J_f||t^J||J_i\rangle|^2\frac{(2J_f+1)}{(2J+1)} , \tag{3.29}$$

where $F_{\rm kin}$ is a kinematical factor, so that the new summation variable J_1 now plays the role of the true nuclear angular-momentum transfer while the old angular-momentum transfer J can differ from it by L. The sum over L (the additional angular-momentum transfer due to nonlocality) is limited because of the rapid convergence of the expansion (3.8) for heavy baryons ($v^{-1}>1$); in practice, $L\lesssim 2$ is sufficient in most cases.

IV. RESULTS FOR THE REACTION $^{14}N(\gamma,\pi^+)^{14}C_{g.s.}$

In this section we study in detail the effect of nonlocality in the reaction $^{14}N(\gamma,\pi^+)^{14}C_{g.s.}$ at pion laboratory kinetic energies 20, 50, and 120 MeV. We have chosen this nucleus to be our "laboratory case" because of its interesting nuclear structure and the special opportunities it provides for high momentum-transfer reactions, such as (γ,π). Photoproduction of positive pions proceeds here purely through the nuclear $M1$ form factor which has been studied[15] in the (e,e') scattering to the 2.313 MeV excited state of ^{14}N (the isospin partner of the ^{14}C ground state). The β decay of ^{14}C is anomalously slow owing to the famous cancellation in the Gamow-Teller nuclear matrix element, and the form factor behaves in an unusual way[15]: Instead of falling off with the momentum transfer Q, as usual in light nuclei, it rises from an almost zero value at $Q=0$ to a maximum approximately where the first minimum occurs in, say, ^{12}C. The nucleus thus prefers to absorb large momentum transfers. Low-energy photoproduction of pions is usually dominated by the Kroll-Ruderman operator $\vec{\sigma}\cdot\vec{\epsilon}$ which governs the β decay as well; this contribution is now suppressed, though not completely since the momentum transfer involved is relatively large (see our Table I and Fig. 8 of Ref. 2). We expect that the other, usually small, terms of the BL operator will become important, and this is indeed the case as is documented below.

TABLE I. Momentum transfers Q(MeV/c) in the reaction $^{14}N(\gamma,\pi^+)^{14}C_{g.s.}$ at different pion laboratory kinetic energies and scattering angles.

	$\theta=20°$	$\theta=90°$	$\theta=180°$
$T_\pi=20$ MeV	80	180	235
$T_\pi=50$ MeV	60	230	315
$T_\pi=120$ MeV	40	340	470

In terms of the nuclear structure input, we have used, as in Ref. 2, the MIT-NBS phenomenological wave functions.[15] At this stage we are not concerned[16] with their unusual physical character since the $T=1$ $M1$ form factor is here the only one contributing to the reaction and hence the nuclear wave functions can be thought of only as a compact way of parametrizing the experimental form factor. Nevertheless, in the future we intend to improve the nuclear structure input, especially with regard to the latest (e,e') measurements. In all our calculations we employ the MSU(79) optical potential[13] as it turns out to be easier to mock with the separable model; only at $T_\pi=20$ MeV have we used the later potential MSU(80) which has been fitted to both scattering and pionic-atom data. Throughout our work we use the separable-model mock pion wave functions fitted to the MSU wave functions, as described in Appendix A. By comparing the nonlocal results with the local ones obtained with the same (mock) pion wave functions, we are able to see the pure effect of the nonlocality. For comparison, we also show the local results for the optical-model wave functions. The difference between the two local results, which is always rather small, illustrates the uncertainty due to the imprecisions in the wave functions. We use the traditional pseudovector (PV) pion-nucleon coupling, except where explicitly indicated otherwise by the label PS.

In Fig. 3 we present the differential cross section calculated at $T_\pi=50$ MeV with the full BL amplitude. The nonlocal results are shown by the two solid curves labeled PV and PS corresponding to the two pion-nucleon couplings and by the dotted curve, which does not contain the contribution of the Δ diagram. As discussed in Sec. II, the band between these three curves reflects our theoretical uncertainty. The dashed curve displays the local mock result while the dotted-dashed curve corresponds to the optical-model (local, of course) calculation. The difference between these two curves is here larger than in most other cases because of the unusual prominence that the pion-pole term gains in ^{14}N. Indeed, the pion-pole term couples only to the derivative of the pion wave function [due to the pion electromagnetic vertex $e(q+q')$], and, as we discuss in Appendix A, the derivatives in the

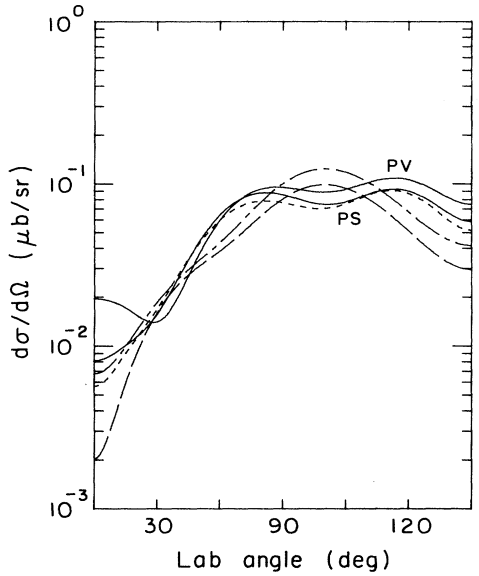

FIG. 3. Differential cross section for the reaction $^{14}N(\gamma,\pi^+)^{14}C_{g.s}$ at pion laboratory energy $T_\pi=50$ MeV. The two solid curves labeled PV and PS correspond to full nonlocal calculating in the PV and PS pion-nucleon couplings. The dotted curve (PV coupling) omits the Δ diagram. The dotted-dashed and dashed curves are calculated in the local limit with the optical-potential (Ref. 13) and mock pion wave functions, respectively.

nonlocal-equivalent case always differ more from their local counterparts than the wave functions themselves.

We start our study of the nonlocalities with the pion-pole term. In Fig. 4 we show its contribution calculated at $T_\pi=50$ MeV both in the local limit (dashed curve) and including the full nonlocality (solid curve). As we expect from the plane-wave considerations of Sec. III A, the effect is large. The peak in the differential cross section is indeed shifted to forward angles in accordance with the plane-wave factor (3.10) which provides a qualitative explanation of the pion nonlocality in all the nuclei studied. In ^{14}N, however, the pion-pole cross section has an additional interesting feature, viz., the second maximum at $\theta=120°$, which cannot be understood from plane-wave considerations. We trace this peak to the unusual behavior of the form factor $F(Q)$ which in ^{14}N rises with the momentum transfer $\vec{Q}=\vec{q}_0-\vec{k}$ (where $\vec{q}_0$ and $\vec{k}$ are the pion and photon momenta the angle between which is the scattering angle θ) instead of falling as it does in all the other cases. The shape of $F(Q)$ as the function of θ can be seen from the contribution of the contact term which follows the form factor rather closely (cf. the dotted-dashed curves in Fig. 4 and in Fig. 15 below for the reaction in ^{13}C. We can explain the second peak in a rather qualitative way by thinking of the momentum-space pion wave function as a diffraction pattern around the asymptotic momentum q_0 and approximating the first two maxima by δ functions,

$$\psi_\pi(\vec{q})\simeq\delta(\vec{q}-\vec{q}_0)+F\delta(\vec{q}-\vec{q}_1)\ . \tag{4.1}$$

The momentum q_1 is then the "first harmonic" and F is a "scattering amplitude." When smeared according to (3.4) and multiplied by the form factor, each of the two δ functions produces a broad peak; the interference between them results in the two-humped shape of the cross section. The effect thus depends importantly on the ability of the form factor to preserve and amplify high Fourier com-

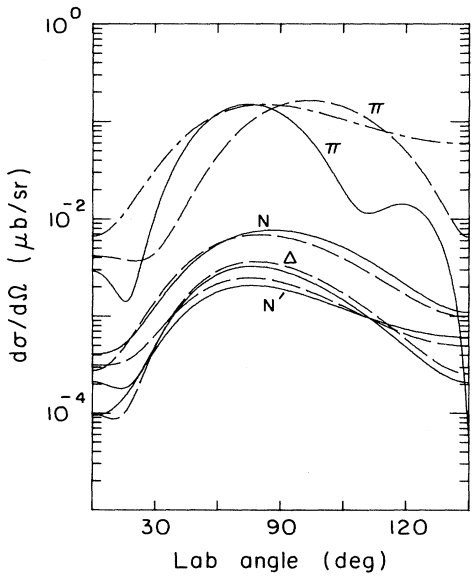

FIG. 4. Contributions of separate Feynman diagrams of Fig. 1 to the differential cross section for the reaction $^{14}N(\gamma,\pi^+)^{14}C_{g.s.}$ at $T_\pi=50$ MeV in the nonlocal case (solid curves) and in the local limit (dashed curves). The dotted-dashed curve is the result for the (always local) contact term.

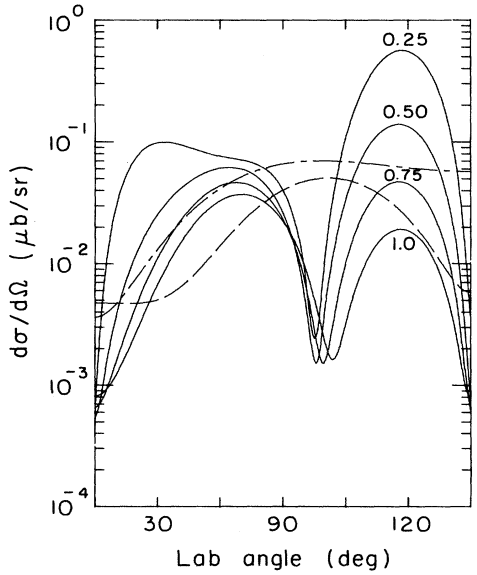

FIG. 5. The dependence of the contribution to $^{14}N(\gamma,\pi^+)^{14}C_{g.s.}$ at $T_\pi=20$ MeV of the nonlocal pion-pole diagram on the ratio in-the-medium pion mass (solid curves) to the free mass $R=m_\pi^*/m_\pi$. For comparison, the dashed curve shows the local pion-pole contribution and the dotted-dashed curve displays that of the contact term.

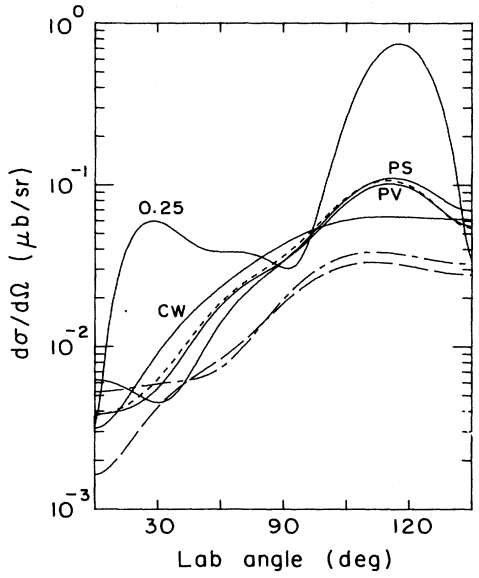

FIG. 6. Same as Fig. 3 but at $T_\pi=20$ MeV. The solid curve labeled 0.25 corresponds to the full result with $m_\pi^*=0.25m_\pi$, while the solid CW curve is obtained in the local limit using only Coulomb pion waves, compared to which the plane-wave results are 20% higher.

ponents hidden in the pion wave function. (To a smaller degree, this effect is also observed in ^{13}C.) Characteristically, at higher energy when the form factor peaks at a smaller angle, the second maximum is less pronounced (cf. Fig. 4 at $T_\pi=50$ MeV and Fig. 5 at $T_\pi=20$ MeV). At even higher energy, $T_\pi=120$ MeV, the second maximum degenerates into a wide plateau. To further explore the pion nonlocality, we soften the in-the-medium pion mass m_π^*, as explained in Sec. II. The solid curves labeled 1.0, 0.75, 0.50, and 0.25 in Fig. 5 are calculated with m_π^* taken as a corresponding fraction of the free mass m_π. Naturally, the nonlocality effect is considerably enhanced when the pion is softened (and vice versa, when m_π^* exceeds m_π, the local limit is approached). It is the already small mass m_π that makes the pion nonlocality so important. The full cross section (cf. Fig. 6) turns out to be rather stable under this change: it is affected appreciably only when $m_\pi^*\lesssim 0.50m_\pi$.

The contributions of the baryonic diagrams of Figs. 1(a), 1(b), and 1(d) are studied at $T_\pi=50$ MeV back in Fig. 4. Their overall strength is almost unaffected by smearing. The nonlocality, however, changes the complex phases of the diagrams. The relative phase ϕ between the nonlocal and local contribution of, say, the N diagram [Fig. 1(a)] is obtained by comparing the interference of this diagram (nonlocal and local) with some other "reference" diagram, e.g., the contact or pion-pole diagram, taken the same (local) in both cases. Only cosines of the angles are obtained in this way; the determination of the angle ϕ thus requires a careful comparison of the results obtained with different reference diagrams. The complex phase ϕ by which the smeared diagram is rotated relative to its local counterpart turns out to be roughly a linear function of the cosine of the scattering angle θ,

TABLE II. Parameters (in deg) of the phase rotation $\phi=a+b\cos\theta$ of the contributions of the smeared diagrams of Fig. 1 relative to their local counterparts.

	$T_\pi=20$ MeV		$T_\pi=50$ MeV		$T_\pi=120$ MeV	
Diagram	a	b	a	b	a	b
N	2	5	5	7	3	6
Δ	2	3	2	3		
π	10	40	30	30		

$$\phi\simeq a+b\cos\theta\ , \tag{4.2}$$

which can be understood simply as the phase

$$e^{i\vec{p}\,\vec{r}}\simeq e^{i(\vec{k}-\vec{q}_0)\vec{r}}\simeq e^{iQr\cos\theta}$$

picked up when the intermediate baryon is allowed to propagate over the distance r. (The initial momentum of the struck nucleon is approximately averaged out.) The coefficient b in (4.2) thus corresponds to the product Qr where Q is some average momentum transfer. A better description would be obtained if Q were made angle dependent, $Q^2=k^2+q_0^2-2q_0k\cos\theta$.

In Table II we present the values of a and b for the direct-nucleon and Δ diagrams at several energies. We found that the linear description (4.2) fits the Δ diagram worse than the nucleon diagram and it completely breaks down at the higher energy $T_\pi=120$ MeV, where the phase starts oscillating with $\cos\theta$. This fact is easy to understand recalling that the Δ denominator provides an additional complex phase which becomes more influential when the energy increases. It is interesting that the coefficient b, which reflects the propagation of the intermediate particle, is almost independent of energy. This was to be expected since the average momentum transfer increases with energy very slowly. The smaller b for the Δ diagram indicates a smaller propagation distance. The same phase

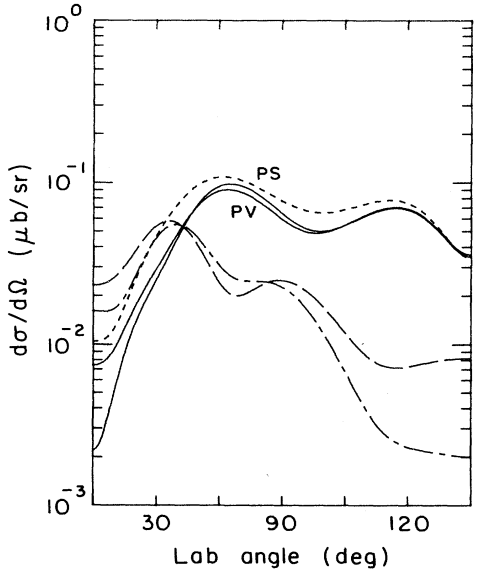

FIG. 7. Same as Fig. 3 but at $T_\pi=120$ MeV.

TABLE III. Total cross sections (μb) corresponding to full nonlocal and local-mock calculations and to separate nonlocal diagrams of Fig. 1.

Reaction	T_π (MeV)	All, local	All, nonlocal	Con.	π	N	N′	Δ
$^{12}C(\gamma,\pi^-)^{12}N_{g.s.}$	43	6.2	6.0	7.2	1.6	0.12	0.05	0.09
$^{12}C(\gamma,\pi^+)^{12}B_{g.s.}$	43	4.7	4.9	6.3	1.8	0.11	0.08	0.07
	140	1.3	1.3	1.5	0.84	0.12	0.10	0.17
$^{14}N(\gamma,\pi^+)^{14}C_{g.s.}$	20	0.24	0.56	0.67	0.22	0.01	0.004	0.004
	50	0.75	0.86	1.3	0.84	0.06	0.02	0.02
	120	0.29	0.76	0.56	0.92	0.06	0.03	0.07
$^{15}N(\pi^+,\gamma)^{15}O_{g.s.}$	50	20	17	21	16	1.2	0.91	2.9
$^{13}C(\pi^+,\gamma)^{13}N_{g.s.}$	50	24	22	25	20	1.4	0.94	3.0
$^{13}C(\gamma,\pi^+)^{13}B_{g.s.}$	43	15	15	14	1.4	0.54	0.22	0.50
$^{13}C(\gamma,\pi^-)^{13}N_{g.s.}$	42	7.3	6.3	6.3	3.9	0.23	0.32	0.72

rotation can also be calculated for the pion-pole diagram (see Table II) for which it is very large, indicating a longer propagation range, which makes the choice of the angle branch of the cosines quite difficult. For this reason there is no π entry at $T_\pi = 120$ MeV in Table II. Note that here the nonlocality strongly affects not only the phase but also the magnitude of the pion-pole contribution (see Fig. 4). The crossed-nucleon diagram [Fig. 1(b)] is affected in a way very similar to the direct diagram. The overall contribution of the baryonic diagrams in ^{14}N is quite small, both relative to the $\vec{\sigma}\cdot\vec{\epsilon}$ term and to the pion-pole term, which is not always the case elsewhere. Our discussion of their nonlocalities, however, remains true in the other nuclei as well. In Fig. 7 we present the results at $T_\pi = 120$ MeV. The nonlocality effect here is very large and, again, it is due mostly to the nonlocality of the pion-pole diagram. These high-energy results, however, are less reliable owing to the deficiency of the small terms of the BL operator (see Sec. II) and since the pion-nucleus wave functions are here less trustworthy (Appendix A).

V. RESULTS FOR THE NUCLEI ^{12}C, ^{13}C, AND ^{15}N AND CONCLUSIONS

In this section we present our results for several other nuclei. We use the same nuclear-structure information as in Refs. 2 and 4 and employ the MSU(79) optical potential[13] to obtain the reference pion wave functions. The PV pion-nucleon coupling is used except where explicitly indicated otherwise. For general orientation, in Table III we summarize the total cross sections for all the reactions both for the full calculations, nonlocal and local mock, and for each separate (nonlocal) diagram. As the inspection of the table shows, the contact diagram CO, which generates only the $\vec{\sigma}\cdot\vec{\epsilon}$ operator and accounts for most of its strength, always yields the largest contribution. The next largest is the pion-pole diagram π, especially in the nonlocal case shown in the table. The baryonic diagrams N, N′, and Δ are much smaller and only influence the details of the differential cross section. It is interesting that the two largest diagrams, CO and π, always interfere destructively, so that the sum cross section is smaller than that of the contact diagram alone. We note that for the PS coupling the all-important role of the contact diagram, the role of producing the Kroll-Ruderman operator and being the largest single contribution, is assumed by one of the nucleon diagrams, N or N′ for the π^+ or π^- photoproduction, respectively.

Table III also reflects some interesting features of the structure of the nuclei investigated. The nucleus ^{12}C is "tight," having closed shells of both protons and neutrons (there is an appreciable configuration mixing, of course), and the $M1$ transition to the 15.11 MeV 1^+ excited state (isospin partner of the ground states of ^{12}B and ^{12}N) proceeds most efficiently through the Gamow-Teller spin and isospin flip operator without any orbital exciations. The contact term is fully dominant here and the other diagrams, which are associated with more complicated operators, are quite small. At the higher energy, $T_\pi = 140$ MeV, these momentum-dependent contributions grow considerably in importance. (As it can also be seen from the reaction on ^{14}N, these terms, especially the Δ, tend to grow with energy, while the contact contribution decreases following the form factor.) By contrast, the nuclei ^{13}C

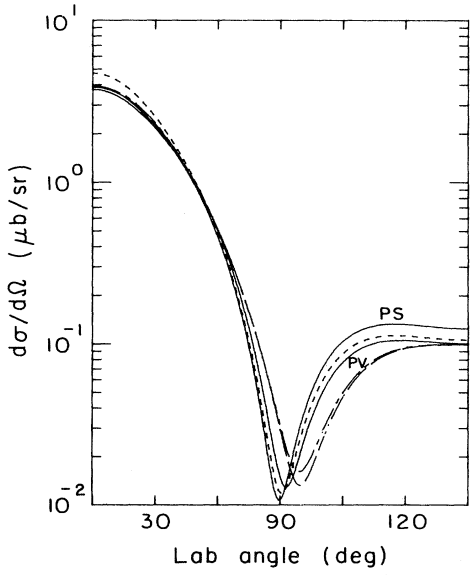

FIG. 8. Same as Fig. 3 but for the reaction $^{12}C(\gamma,\pi^-)^{12}N_{g.s.}$ at $T_\pi = 43$ MeV.

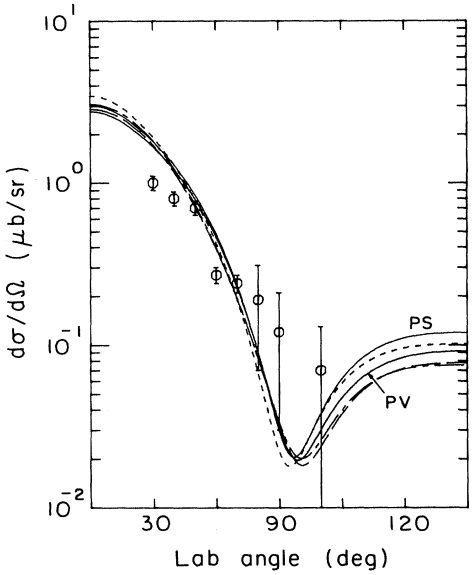

FIG. 9. Same as Fig. 3 but for the reaction $^{12}C(\gamma,\pi^+)^{12}B_{g.s.}$ at $T_\pi=43$ MeV. The data are from Ref. 18.

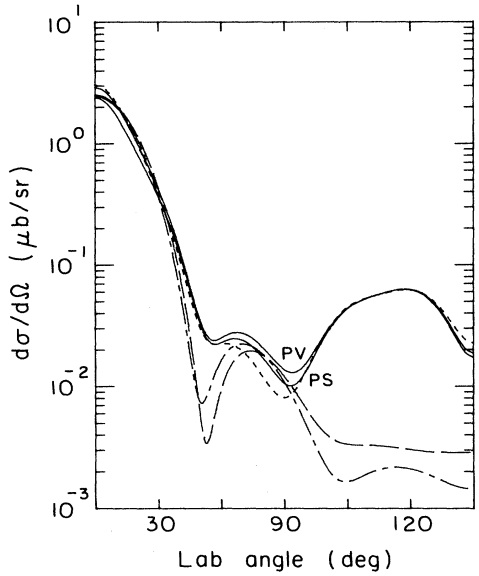

FIG. 10. Same as Fig. 9 but at $T_\pi=140$ MeV.

and ^{15}N are "loose," having a valence neutron (or a hole) which allows them to respond to various spin and orbital angular momentum operators associated with the small diagrams of Figs. 1(a)—1(d). Indeed, these contributions are an order of magnitude larger than in ^{12}C. The contact-diagram cross section is also increased, reflecting the allowed Gamow-Teller transition between mirror nuclei relative to a particle-hole excitation, but the increase is not as dramatic as for the other diagrams and the Kroll-Ruderman term here appears as relatively "suppressed." It is telling that photoproduction of negative pions on ^{13}C is quite similar to that on ^{12}C since it takes place only on protons whose configurations are the same in both cases.

The differential cross sections are presented in Figs. 8—15. As before, the nonlocal results are shown by the two solid curves labeled PV and PS and by the dotted curve which we calculate omitting the Δ diagram. As discussed above, the band between these three curves reflects the theoretical uncertainty (our "best bet" is the dotted curve). For comparison, the local results are also shown by the dashed curve (mock pion wave functions) and dotted-dashed curve (the reference optical-model functions).

Figures 8 and 9 display the results for the reactions $^{12}C(\gamma,\pi^-)^{12}N_{g.s.}$ and $^{12}C(\gamma,\pi^+)^{12}B_{g.s.}$ at $T_\pi=43$ MeV. The Kroll-Ruderman term is here dominant (see Table III) so that the nonlocality cannot have any appreciable effect in either coupling. Indeed, all the calculated curves are close to one another. In the resonance region (Fig. 10), however, the back angles are affected quite strongly, since the $\vec{\sigma}\cdot\vec{\epsilon}$ term has already died off with the form factor; the effect is due almost entirely to the pion nonlocality. The (γ,π^+) results are in a reasonable agreement with the 43 MeV data[18] although the shape of the differential cross section is not reproduced too well and the theory seems to be too high at forward angles.

The other nuclei are more interesting. In Figs. 11 and 12 we deal with the reaction of the radiative capture (π^+,γ) to the ground state on the nuclei ^{15}N and ^{13}C. The Kroll-Ruderman term is here suppressed and it interferes[4] with the pion-pole term producing a minimum in the differential cross section around 90°. The nonlocality turns this minimum into a shoulder with a marked difference between the two pion-nucleon couplings. The omission of the Δ diagram, following our arguments in Sec. II, restores the minimum and shifts it somewhat to forward angles. (In a local counterpart of the dotted curves the minimum is more pronounced.)

Finally, in Figs. 13 and 14 we show the differential

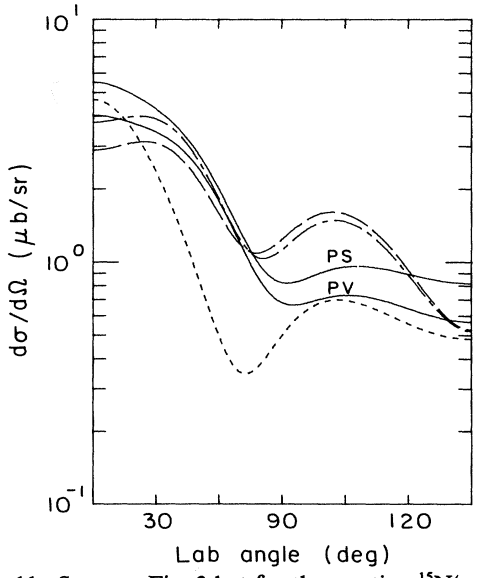

FIG. 11. Same as Fig. 3 but for the reaction $^{15}N(\pi^+,\gamma)^{15}O_{g.s.}$ at $T_\pi=50$ MeV.

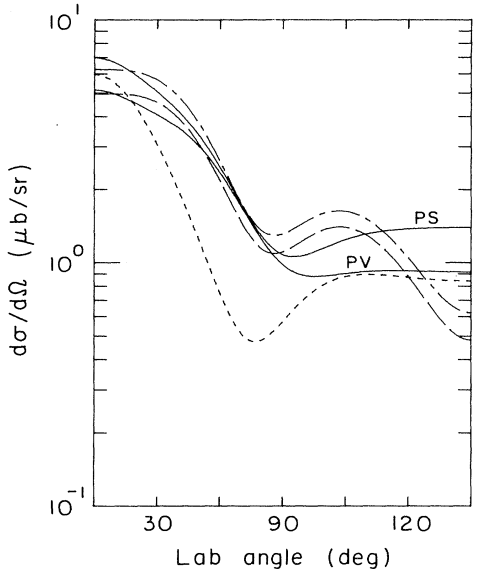

FIG. 12. Same as Fig. 3 but for the reaction $^{13}C(\pi^+,\gamma)^{13}N_{g.s.}$ at $T_\pi=50$ MeV.

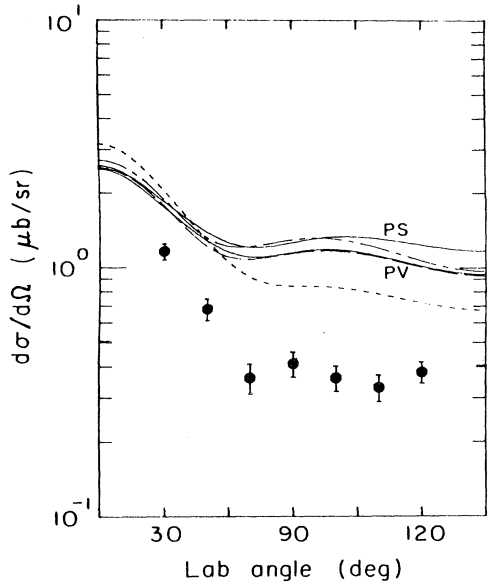

FIG. 14. Same as Fig. 3 but for the reaction $^{13}C(\gamma,\pi^+)^{13}B_{g.s.}$ at $T_\pi=43$ MeV. The data are from Ref. 5.

cross sections for the reactions $^{13}C(\gamma,\pi^-)^{13}N_{g.s.}$ and $^{13}C(\gamma,\pi^+)^{13}B_{g.s.}$. It is in these reactions that the largest discrepancies with experiment were discovered.[5] Here, all the usually-small diagrams π, N, N′, and Δ produce comparable and relatively large contributions (see Table III and Fig. 15), so that the nonlocality is both large and difficult to delineate. The calculated results, both local and nonlocal, are well above the data. In this case, however, the nuclear structure input (Cohen-Kurath wave functions[16] have been used) is clearly inadequate since the calculated electron-scattering form factors are considerably higher than the experimental ones.[15] Unfortunately, a simple adjustment of the wave functions, the way it has been done for ^{14}N, cannot be performed here since the $T=1$ information required in the photopion reactions is not measured directly; even more so, an overall rescaling of the Cohen-Kurath form factors to the electron scattering data proves to be not sufficient to bridge the order of magnitude gap between the photoproduction theory and experiment. Thus a thorough nuclear-structure calculation is needed to explain the drastic suppression of the form factors. It has been suggested that this effect arises from core polarization.[19] Others claim that it is due to pion condensation.[8] Their results, however, are not in the form that can be directly used in our calculations.

To summarize, we have made our best effort to faithful-

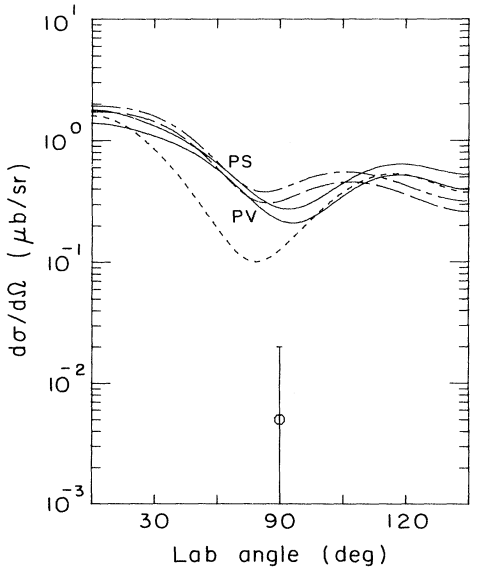

FIG. 13. Same as Fig. 3 but for the reaction $^{13}C(\gamma,\pi^-)^{13}N_{g.s.}$ at $T_\pi=42$ MeV. The data point is from Ref. 5.

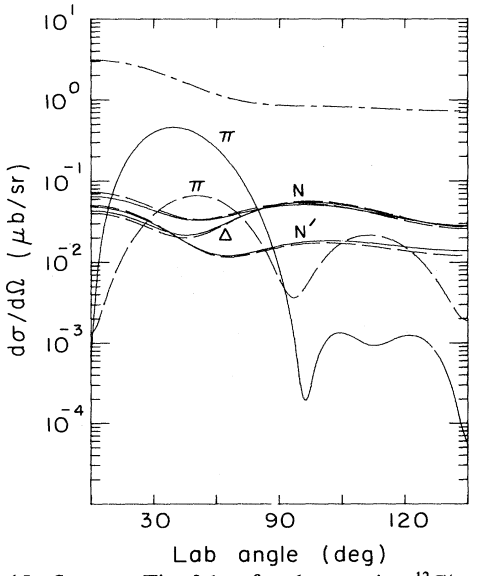

FIG. 15. Same as Fig. 3 but for the reaction $^{12}C(\gamma,\pi^+)^{12}B_{g.s.}$ at $T_\pi=43$ MeV.

ly implement the one-body operator approach (OBOA) to nuclear photopion reactions using the best available nuclear-structure and pion-nucleus information. With the introduction of nonlocalities there are no significant calculational approximations left and the remaining (and arising) disagreements with data must be attributed to inadequate ingredients or to many-body operators. More work needs to be done providing a better BL-type photoproduction operator, better pion-nucleus wave functions, preferably obtained in a momentum-space calculation, better nuclear-structure information, especially for the reactions on ^{13}C, and, finally, introducing the Pauli blocking in a proper way.[17] Once the remaining discrepancies are resolved in the "simple cases," such as $^{12}C(\gamma,\pi^+)^{12}B_{g.s.}$, photopion calculations may become reliable enough to provide a complementary source of information both on pion-nucleus interactions and on nuclear $T=1$ form factors. With such new, hopefully forthcoming, calculations and high-precision measurements the subject is out of its infancy.

ACKNOWLEDGMENTS

The authors thank Prof. J. M. Eisenberg, Prof. S. Gurvitz, and Prof. C. M. Vincent for their helpful comments. This work was supported in part by the U.S. National Science Foundation under Contract PHY-7920762.

APPENDIX A: PION-NUCLEUS MOCK WAVE FUNCTIONS

To make the Fourier-Bessel transform (3.16) possible, we replace the previously used[2,4] MSU optical-potential wave functions[9] by model pion-nucleus functions which can be transformed and which mock the behavior of the original functions in the inner region. For computational ease we have chosen the model as a rank-one separable potential in each partial wave,

$$v(p,p')=g(p)\frac{\lambda}{\pi\mu}g(p') \tag{A1}$$

with a complex (energy-dependent) strength λ. As is well known, the scattering amplitude is then

$$f=-t_{q_0}(q_0,q_0)=-g(q_0)\frac{1}{1/\lambda+R(q_0)}g(q_0)\ , \tag{A2}$$

where

$$R(q_0)=\frac{2}{\pi}\int_0^\infty \frac{g^2(q)q^2dq}{q^2-q_0^2-i\epsilon} \tag{A3}$$

and the outgoing scattering wave function in momentum space is

$$\psi_{q_0}^{(+)}(q)=\frac{\delta(q-q_0)}{q_0^2}+\frac{2}{\pi}\frac{t_{q_0}(q,q_0)}{q^2-q_0^2-i\epsilon}$$
$$=\frac{\delta(q-q_0)}{q_0^2}+F(q_0)\frac{g(q)}{q^2-q_0^2-i\epsilon}\ . \tag{A4}$$

Performing the transform to coordinate space we obtain

$$\phi(r)=\frac{2}{\pi}\left[j_l(q_0r)+F(q_0)\int_0^\infty \frac{q^2j_l(qr)g(q)dq}{q^2-q_0^2-i\epsilon}\right]\ . \tag{A5}$$

We have chosen the form factors $g(q)$ to be linear combinations of two Yamaguchi or Gaussian terms,

$$g(q)=g_1(q)+\gamma g_2(q) \tag{A6}$$

with a complex γ and

$$g_i(q)=q^{l_i}/(q^2+\beta_i^2)^{l_i+1} \tag{A7}$$

or

$$g_i(q)=q^{l_i}e^{-\alpha_i q^2}\ . \tag{A8}$$

The Yamaguchi form (A7) was used in the calculations; the Gaussian form leads to similar results.

The coefficient $F(q_0)$ and the overall normalization are obtained by matching the function (A5) and its derivative to the reference function at some matching distance R taken as 6 fm for p shell nuclei. Our mock functions are thus automatically phase shift equivalent to the original wave functions and there is no need to calculate the strength parameter λ. The remaining parameters of the form factors β_i, l_i, and γ are adjusted so as to reproduce the reference wave functions in the internal region as well as possible. The Coulomb interaction is taken into account implicitly, since we fit to a Coulomb-containing function. In fact, since we match at a distance which is too large to be probed in photopion reactions, our procedure is an equivalent of the Vincent-Phatak method[12] for treating the Coulomb tail in momentum-space calculations.

The fit is rather good as can be seen from Figs. 16 and 17 which show the s-wave mock wave functions for the reaction $^{14}N(\gamma,\pi^+)^{14}C_{g.s.}$ at $T_\pi=50$ and 120 MeV. It is only slightly worse for higher partial waves. Note that we fit only the wave functions themselves so that the derivatives are reproduced with somewhat less precision. In ad-

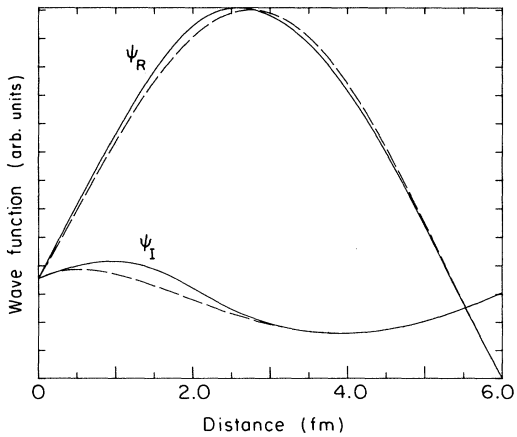

FIG. 16. The pion wave function for the reaction $^{14}N(\gamma,\pi^+)^{14}C_{g.s.}$ at $T_\pi=50$ MeV. The solid curves are obtained using the MSU(79) optical potential (Ref. 9), and the dashed curves are the mock pion waves (see Appendix A).

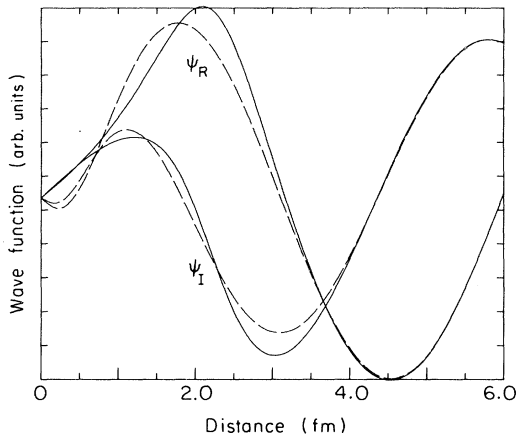

FIG. 17. Same as for Fig. 16, but at $T_\pi = 120$ MeV.

dition, the derivatives of the MSU optical functions contain discontinuities which are due to the unbounded term $\vec{\nabla}\cdot\rho\vec{\nabla}$ in the optical potential. These kinks are more pronounced in the p and d partial waves and at higher energies. The mock wave functions smooth these discontinuities and, thus, are more physical in this respect.

The main difference between the mock and reference wave functions is that the former contain a higher degree of nonlocality. We recall here the Perey effect[20]: for a real attractive interaction a nonlocal equivalent of a local wave function tends to be suppressed in the interior region reflecting the flux going to the other channels implicitly present in the nonlocal case; for a repulsive interaction the converse is true. This tendency becomes quite pronounced in the resonance region where the strong absorption simulates repulsion. In fact, to overcome this effect at $T_\pi = 120$ MeV, our mock function developed an additional node very close to the origin (Fig. 17).

We wish to point out that the suppression is not very strong even in the resonance region (approximately a factor of $\sqrt{2}$ in the amplitude) so that the familiar motto "pions do not penetrate into nuclei" is termed too strongly. In fact, the "true" pion wave function is, most probably, even less suppressed since the optical potential underestimates the nonlocality. The photopion reactions probe the pion wave function inside the nucleus and thus much more reliable wave functions are needed for the (γ,π) calculations in the resonance region.

Finally, we note that even the optical-potential wave functions are nonlocal to some extent because of the presence of the derivative-dependent interaction. This can be explicitly seen by considering the radial current

$$j_R(r) = (r\psi)^* \overleftrightarrow{\partial}_r (r\psi) \ . \tag{A9}$$

Writing

$$u = r\psi = |u| e^{i\varphi} \ , \tag{A10}$$

we obtain

$$j_R(r) = |u|^2 \frac{d}{dr}\varphi \ . \tag{A11}$$

For a local absorptive potential $V = U - iW$, $W > 0$, the radial divergence of the current is negative,

$$D \equiv \frac{d}{dr} j_R = -w(r)|u|^2 \ , \tag{A12}$$

which is no longer true if the interaction is nonlocal. Plots of the divergence for the optical pion-nucleus wave functions clearly display "creation regions" inside the nucleus, i.e., regions where $D > 0$. For the mock wave functions these regions are more pronounced. Of course, such regions appear for nonlocal potentials only inside the nuclei, reflecting the redistribution of flux. On the nuclear surface the divergence D is always negative, as appropriate for net physical absorption.

APPENDIX B: NUMERICAL PROCEDURES

We discuss here the numerical evaluation of the integrals $I_{lLl_1}(r)$ given by (3.7) and (3.15). In the pion-pole case (3.7) the integral presents a twofold difficulty: the pole singularity of the scattering wave function (A4) and rapid oscillations of the Bessel function $j_l(pr)$, especially at large r. To avoid the pole, we make use of the analyticity of the form factors and calculate the integral along a complex path around the singularity at $q = q_0$. In the case of the Yamaguchi form factors (A7) the path is subsequently deflected into the upper complex half plane, after having replaced the j_l by $\mathrm{Im}(h_l^+)$ which turns the oscillations into damped exponentials.[21] For the baryon case (3.15), there is no pole and the function R falls off quite rapidly, so that the integral is easily calculated along the real axis. Because of the oscillations of the j_l, we use the trapezoidal rule which works here much better than the Gauss rule, especially at high l. We thank Dr. H. Amakawa for his advice on this subject.

In calculating the integral (3.7), we separate out the plane-wave part of the pion wave function,

$$\psi_\pi(\vec{x}) = \psi_\pi^{\mathrm{PW}}(\vec{x}) + \psi_\pi^D(\vec{x}) \tag{B1}$$

and smear it explicitly by the formula (3.10); the remaining distorted part $\psi_\pi^D(\vec{x})$ contains only a limited number of partial waves, which truncates the angular-momentum summations.

Finally, the Legendre functions $Q_L(z)$, which are needed for both real and complex arguments, can be easily calculated from their hypergeometric series when the argument is not too close to unity. In the difficult case $z \simeq 1$, we first calculate the ratio

$$R_L(z) = \frac{Q_L(z)}{Q_{L+1}(z)} \tag{B2}$$

using the upward recurrence relation

$$R_L(z) = \frac{L+1}{z(2L+1) - LR_{L-1}(z)} \ . \tag{B3}$$

Then, we iterate down the Legendre functions themselves starting from $Q_{L+1} = 1$ and $Q_L = R_L$,

$$Q_{L-1}(z) = \frac{2L+1}{L} z Q_L(z) - \frac{L+1}{L} Q_{L+1}(z) \ , \tag{B4}$$

which is a stable procedure. Once $L=0$ is reached, the sequence is renormalized referring to

$$Q_0=\tfrac{1}{2}\ln[(z+1)/(z-1)] .$$

It turns out that iterating up the ratios R_L is a much more stable procedure than iterating up the functions Q_L. Indeed, for $L \lesssim 8$ it can be used up to $z \simeq 1.5$, at which point the hypergeometric series already converges sufficiently quickly.

---

*Present address: Department of Nuclear Physics, The Weizmann Institute of Science, Rehovot 76100, Israel.

[1]W. C. Haxton, Phys. Lett. 92, 37 (1980); V. de Carlo and N. Freed, Phys. Rev. C 25, 2162 (1982); A. Nagl and H. Überall, Phys. Lett. 96B, 254 (1980); V. Girija and V. Devanathan, Phys. Rev. C 26, 2152 (1982); S. Malecki (private communication); and M. V. N. Murthy, G. Ramachandran, and S. K. Singh, University of Mysore report, 1982. Earlier propagator nonlocality studies appear in A. Figureau and N. C. Mukhopadhyay, Nucl. Phys. A338, 514 (1980), and in Ref. 10.

[2]M. K. Singham and F. Tabakin, Ann. Phys. (N.Y.) 135, 71 (1981); M. K. Singham, Ph.D. thesis, University of Pittsburgh, 1980, and references therein. Also see F. Tabakin, Proceedings of the Symposium on Medium Energy Physics and Nuclear Structure, Madras, 1983 (to be published).

[3]A. Nagl, F. Cannata, and H. Überall, Acta. Phys. Austriaca 48, 267 (1976); R. Graves *et al.*, Can. J. Phys. 58, 48 (1980). Experiments on pion radiative capture in flight are presently underway by K. Crowe, C. J. Martoff, J. Deutsch, and P. Truöl (private communications).

[4]G. W. Reynaud and F. Tabakin, Phys. Rev. C 23, 2652 (1981); G. W. Reynaud, Ph.D. thesis, University of Pittsburgh, 1982.

[5]A. M. Bernstein, *An Introduction to* (γ,π) *Reactions, Lectures at International School of Intermediate Energy Nuclear Physics,* edited by R. Berger, S. Costa, and C. Schaerf (World Scientific, Singapore, 1982). N. Paras *et al.*, Phys. Rev. Lett. 42, 1455 (1979); J. J. LeRose *et al.*, Phys. Rev. C 25, 1702 (1982); D. Rowley *et al.*, *ibid.* 25, 2652 (1982).

[6]S. Dytman (private communication); P. Stoler (private communication); E. C. Booth (private communication); in Report of the Workshop on Future Directions in Electromagnetic Nuclear Physics, Bates Linear Accelerator—MIT, 1981; *Photopion Nuclear Physics,* edited by P. Stoler (Plenum, New York/London, 1979).

[7]I. Blomqvist and J. M. Laget, Nucl. Phys. A280, 405 (1977).

[8]See, for example, *Mesons in Nuclei,* edited by M. Rho and D. Wilkinson (North-Holland, Amsterdam, 1979) Vol. III, or W. Weise, Comments Nucl. Part. Phys. 10, 109 (1981). J. Delorme, A. Figureau, and P. Guichon (unpublished).

[9]M. K. Banerjee and G. E. Walker, Phys. Rev. C 27, 657 (1983).

[10]J. Delorme, M. Ericson, and G. Fäldt, Nucl. Phys. A240, 493 (1975).

[11]J. L. Friar and B. F. Gibson, Phys. Rev. C 15, 1779 (1977).

[12]C. M. Vincent and S. C. Phatak, Phys. Rev. C 10, 391 (1974).

[13]K. Stricker, H. McManus, and J. A. Carr, Phys. Rev. C 19, 929 (1979); K. Stricker, J. A. Carr, and H. McManus, *ibid.* 22, 2043 (1980).

[14]E. J. Moniz, Nucl. Phys. A354, 535c (1981); E. Oset and W. Weise, *ibid.* A329, 365 (1979).

[15]N. Ensslin *et al.*, Phys. Rev. C 9, 1705 (1974); 19, 569 (1979); R. S. Hicks *et al.*, *ibid.* 26, 339 (1982).

[16]D. Kurath (private communication); S. Cohen and D. Kurath, Nucl. Phys. 73, 1 (1965).

[17]E. J. Moniz and A. Sevgen, Phys. Rev. C 24, 224 (1981).

[18]K. Shoda *et al.*, Nucl. Phys. A350, 372 (1980); Phys. Rev. C 27, 443 (1983).

[19]T. Suzuki *et al.*, Nucl. Phys. A358, 421 (1981); Phys. Lett. 106B, 19 (1981); and (to be published). Also see C. K. Lin and L. Zamick, Nucl. Phys. A365, 411 (1981).

[20]N. Austern, Phys. Rev. 137, B752 (1965).

[21]C. M. Vincent and H. T. Fortune, Phys. Rev. C 2, 782 (1970).